Journal of Membrane Science Letters 5 (2025) 100099

Contents lists available at ScienceDirect

Journal of Membrane Science Letters

journal homepage: www.elsevier.com/locate/memlet

Partition energy in polyamide membranes and its link to ion-ion selectivity

Liat Birnhack [a,1], Oren Ben Porat [a,1], Ori Fridman [a], Tiezheng Tong [b], Razi Epsztein [a,*]

[a] Faculty of Civil and Environmental Engineering, Technion – Israel Institute of Technology, Haifa 32000, Israel
[b] School of Sustainable Engineering and the Built Environment, Arizona State University, Tempe, AZ, 85287, United States

ARTICLE INFO

Keywords:
Reverse osmosis
Ion transport
Ion dehydration
Energy barrier
Quartz crystal microbalance

ABSTRACT

Understanding the mechanisms of molecular transport in polyamide membranes is imperative to improve their solute-specific selectivity. We explored the partitioning behaviors of water and salts in polyamide membranes to elucidate the role of ion-membrane interactions in the transport. Quartz crystal microbalance (QCM) was employed to quantify the mass uptake at different temperatures and determine partition energies (E_k) for water and salts under two different pH values. Zeta potential and permeability tests were conducted to support the ion-membrane affinity trends observed with QCM and link these trends to ion-ion selectivity. Our results demonstrate a high affinity of water to the polyamide membrane ($E_k < 0$), with a significant swelling effect attributed to dipole interactions and hydrogen bonding. Ion partitioning revealed distinct differences between monovalent and divalent cations, as well as between kosmotropic and chaotropic anions. Specifically, divalent cations (Ca^{2+} and Mg^{2+}) exhibited considerably lower partition energies (-0.99 and 0.29 kcal mol^{-1}, respectively) and more efficient charge neutralization, indicating stronger interactions with the membrane compared to monovalent cations (~2.2 kcal mol^{-1}). The partition energies of the chaotropic iodide and kosmotropic sulphate anions were substantially different (-5.5 and 4.0 kcal mol^{-1}, respectively), likely due to the different tendency of these anions to shed their hydration shell and stick to the polymer. Last, our permeability tests indicate the potential existence of an intrinsic tradeoff between ion partitioning and intrapore diffusion, presumably due to the opposite effects that ion-membrane interactions have on these transport steps. Overall, our work underscores the role of ion-specific interactions in membrane transport and selectivity.

1. Introduction

Molecular-level interactions that govern water and solute permeation through polyamide (PA) reverse osmosis (RO) and nanofiltration (NF) membranes have been a focal point of research in recent years (Heiranian et al., 2022; Ridgway et al., 2017; Nickerson et al., 2022). This field primarily builds on the widely accepted solution-diffusion model (Wijmans and Baker, 1995; Paul, 2004; Heiranian et al., 2023; Chen et al., 2021) or other related transport models (Fan et al., 2024; Mai et al., 2019; Wang et al.; 2023; Wang et al., 2014; Wang et al., 2021; Kimani et al., 2021; Yaroshchuk et al., 2013; Hu et al., 2023; Vickers et al., 2025; Wang and Lin, 2021), which provide a foundational framework for understanding transport through these membranes. Despite significant advances in elucidating membrane transport mechanisms within this framework, certain mechanism aspects remain poorly understood (Fan et al., 2024; Shefer et al., 2021; Wang et al., 2022). Bridging these knowledge gaps is essential for designing membranes with enhanced solute-solute selectivity, which could lead to substantial improvements in water treatment and resource recovery applications (Zhu et al., 2021; Jin et al., 2022; Zhao et al., 2021; Razmjou et al., 2019; Epsztein, 2022; Sujanani et al., 2020; Tang and Bruening, 2020).

Current theories on solute partitioning to and diffusion through polyamide membranes propose that each of these steps is influenced by a range of factors, including electrostatic interactions, steric hindrance, and other effects impacting the inherent affinity of the transporting solute to the membrane material (Nickerson et al., 2022; Chen et al., 2021; Shin et al., 2022; Ghoufi et al., 2017; Drazevic et al., 2012; Pavluchkov et al., 2022; Bannon et al., 2024; Bannon and Geise, 2024; Geise et al., 2014; Freger, 2023; Yazzie et al., 2024; Yaroshchuk, 2001). For ions, specific properties—such as valence, hydrated size, and hydration energy—play essential roles in determining partitioning to the PA layer and diffusion within it (Nickerson et al., 2022; Roth et al., 2024). The effective energy barriers for the transport of different ions through various PA membranes, which account for both the partition energy and

* Corresponding author.
E-mail address: raziepsztein@technion.ac.il (R. Epsztein).
[1] These authors contributed equally to this work

https://doi.org/10.1016/j.memlet.2025.100099
Received 14 March 2025; Received in revised form 28 April 2025; Accepted 29 April 2025
Available online 2 May 2025

energy barrier for intrapore diffusion, were quantitatively determined in recent publications (Zhou et al., 2020, Rickman et al., 2014; Gao et al., 2015; Schwindt et al., 2024; Kingsbury et al., 2024). However, attempts to link these effective energy barriers to the ability of the membrane to selectively separate ions showed poor correlation, highlighting the need for in-depth exploration of the energy landscape of transport through the membrane, e.g., understanding this landscape in terms of partition energy and energy barrier for diffusion (Zhou et al., 2020; Shefer et al., 2022).

The current study systematically investigates the partition enthalpy (E_k, referred to in the text, for simplicity, as partition energy) of water and different salts in a commercially available PA RO membrane as a primary indicator for their affinity to the membrane and a major component in the energy landscape of transmembrane permeation. To quantify the E_k of water and these salts, we used quartz crystal microbalance (QCM) under different conditions, adjusting previously reported methods that measured salt partition in PA membranes (Wang et al., 2021; Wang et al., 2017; Lin et al., 2018; Freger, 2004; Villalobos et al., 2023; Dunmyer et al., 2024). We then explored the permeation of the ions in pressurized filtration to link the values of partition energy to ion permeability and ion-ion selectivity. Our results suggest that both the ion hydration strength (for anions) and ion-membrane electrostatic interactions (for cations) affect the ion affinity to the membrane. Notably, our permeation tests introduce a more complex picture of ion-ion selectivity, which cannot be explained by the partition enthalpy alone.

2. Materials and methods

2.1. Membranes and chemicals

Flat sheets of a thin-film composite polyamide RO membrane (SW30HR, FilmTec) were used for all experiments. Analytical grade chloride-based salts (CsCl, NaCl, LiCl, $CaCl_2$, and $MgCl_2$), as well as sodium-based salts (NaI, NaCl, and Na_2SO_4) were purchased from Fisher Chemicals, Merck, and BioLab. Hydrochloric acid (HCl) and sodium hydroxide (NaOH) of 0.05 M were used to adjust pH. Deionized water (DIW) (Zailon, < 0.8 μS cm^{-1}) was used in the pressure filtration system, while ultrapure water (Merck, < 0.055 mS cm^{-1}) was used in the QCM, zeta potential, and ion chromatograph analyses. For the QCM experiments, the membranes were soaked in a 99.9% v/v isopropyl alcohol (Biolab Chemicals) before the coating procedure. Dimethylformamide at a concentration of 99.5% w/w (Biolab Chemicals) was used to dissolve the polysulfone layer from the membrane.

2.2. Determination of partition energy using quartz crystal microbalance

To measure interactions between the solution and the polyamide layer of the RO membrane solely, which is the relevant layer affecting the transport in polyamide membranes, we used a quartz crystal microbalance (QSense Analyzer, Biolin) that enables the detection of mass changes on the QCM sensor in the nanogram scale. We first separated the PA from the support layer and adhered it to the QCM sensor by adopting and tweaking a previously reported procedure (Supporting Information) (Freger, 2004). Each deposited PA layer was used for a single experiment, after which the sensor was rinsed and cleaned. We initially used the QCM to measure the mass of the deposited polyamide layer. We then used the same coated sensors for determining the partition energy of DIW and various salts. The sensors were first exposed to DIW across six descending temperatures, from 34°C to 14°C. We chose to conduct all the experiments in descending temperature order since it assures stabilization of the polyamide at the maximal temperature (Allouzi et al., 2025). Each temperature was maintained for at least 25 minutes, allowing the system to stabilize (with $\Delta f < 2$ Hz over 10 minutes). Last, the sensors were exposed to a 1.0 N single-salt solution following the same temperature profile. (Sujanani et al., 2023) We acknowledge that the formation of ion pairs, such as $NaSO_4^-$ and $MgCl^+$, is not negligible and may impact the extent and the nature of partitioning, as we discuss in section 3.2 (Sujanani et al., 2023; Fisher and Fox, 1975; Broadwater et al., 1976)

For all tests, three coated sensors were placed in the QCM modules alongside an uncoated control sensor to account for the effects of viscosity and density on the frequency (Arrizabalaga et al., 2025). During all steps, a flow rate of 0.15 ml min^{-1} was applied. By the end of the experiment, we obtained frequency data of the three sensors before and after coating, and upon exposure to DIW and salt solutions at six different temperatures, along with the corresponding control sensor data. For each specific stage, an averaged frequency, based on measurements taken over the final three minutes of the stage, was taken for further calculation of the partition energy, as described in detail in the Supporting Information.

2.3. Zeta potential measurements

To support the QCM results, we also evaluated the ion affinity to the membrane by measuring the zeta potential (ZP, ζ) of the membrane surface using the streaming potential method with SurPASS3 electro kinetic analyzer (Anton Paar GmbH, Austria). For the ZP measurements, five chloride-based single salt solutions (i.e., LiCl, NaCl, CsCl, $MgCl_2$, and $CaCl_2$) at a concentration of 1.0 mN (i.e., 1.0 charge-based meq/L) were used. We chose to keep the charge-based equivalent concentrations constant (i.e., 0.5 mM for each divalent-based salt and 1.0 mM for each monovalent-based salt) rather than constant molar concentrations in order to attain the same charge of the ions that are compared in the examination. The same strategy was used also in the partitioning and filtration experiments. More information on the ZP measurement is provided in the Supporting Information.

2.4. Membrane permeability tests

The experimental crossflow filtration setup used for the permeability tests and the permeability calculations are described in the SI. The applied pressure, crossflow velocity, and temperature were continuously monitored and maintained constant. Mixed solutions of chloride-based salts (i.e., LiCl, NaCl, CsCl, $MgCl_2$, and $CaCl_2$, 2.0 mN each) or sodium-based salts (NaI, NaCl, and Na_2SO_4, 2.0 mN each) were used at pH of 6.0 and 4.0. We note that the salt concentration in the QCM tests was much higher compared to the concentration in the filtration and ZP experiments due to technical limitations and the specific requirements of each testing protocol. Notably, the relatively high salt concentration used in the QCM tests aimed to increase the detection and accuracy of frequency measurements under the specific conditions applied in this work. The consequences of such differences in salt concentration across different tests are further discussed in the Results and Discussion. However, our results suggest that despite the different concentrations used in different tests, production of meaningful correlations between these tests is achievable. Ion chromatography (930 Compact IC Flex, Metrohm) was used for measuring feed and permeate concentrations of anions and cations (Metrosep A Supp 7 column and Metrosep C 4 column, respectively). Concentration polarization was taken into consideration using the film theory (Supporting Information) (Wijmans and Baker, 1995; Oren et al., 2021).

3. Results and discussion

3.1. Uptake and partition energy of water

After deposition of the active layer on the QCM sensor (Fig. S1), our first set of experiments aimed to understand the affinity of water to the membrane (Fig. 1). Examining the extent of water uptake by the PA layer deposited on the QCM sensors demonstrates that the polyamide swells considerably (Fig. 1a and Table S1). Specifically, the average water uptake was 0.55 g DIW/g PA with uncertainty of 0.24 g DIW/g PA,

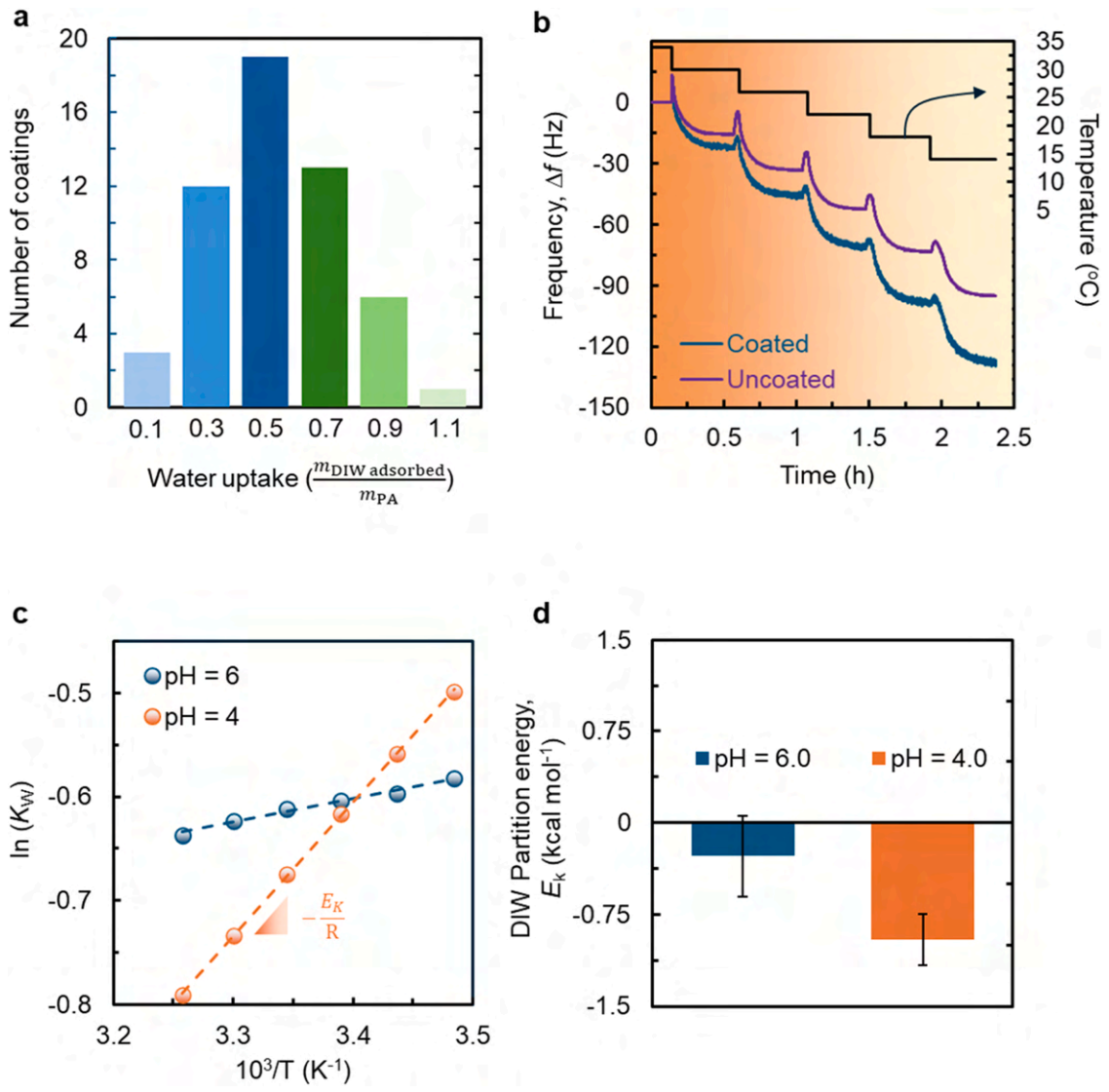

Fig. 1. QCM Measurements of DIW partition energy. (a) Distribution (i.e., number of coatings out of the total 55 coatings tested) of normalized water uptake by the polyamide layer (i.e., mass of water uptake over mass of PA). (b) Representative raw frequency results of polyamide-coated sensor and uncoated sensor when exposed to DIW at descending temperatures. (c) Representative linearization of the van't Hoff equation (Eq. (S10)) for DIW adjusted to pH = 6.0 and 4.0. (d) Average partition energy for water in the SW30HR membrane computed from the slopes of Eq. (S10) for 25 and 6 sets of experiments at pH = 6.0 and 4.0, respectively. The error bars represent standard deviation.

where most coatings (i.e., 82%) showed an increase in mass of between 20% and 80% of the dry polyamide mass. Notably, the results indicate that the polyamide layer of RO membranes has high affinity towards water. To quantitatively determine the membrane affinity towards water, we measured frequency changes due to water uptake as a function of temperature (Fig. 1b) and used Eq. (S1) to convert frequency to mass, Eq (S2) to calculate the mass of the PA layer, and Eqs. (S8) and (S9) to calculate the water partitioning (K_w) at each temperature. We further analyzed the resultant K_w values at descending temperatures to calculate the energy of water partitioning at two different pH levels (Fig. 1c).

Our partition energy results for water, which correspond to the difference in enthalpy of water molecules between the bulk solution and membrane pore, show a slightly negative energy of partition, suggesting that water favors the partitioning into the membrane (Fig. 1d). The water-polyamide interactions comprise hydrogen bonds and electrostatic interactions between water molecules and carboxylic groups present on the membrane. Decreasing the water pH from 6.0 to 4.0 affects both the membrane and water properties, impacting the partition energy of water. Notably, since the pK_a of the carboxylic groups on the membrane is accepted to be between 4.2 and 5.6 (Roth et al., 2024; Chen et al., 2017), pH reduction reduces the fraction of charged carboxylic groups on the membrane, which is expected to hinder water partitioning (Tu et al., 2011). On the other hand, higher hydronium ion concentration in bulk water results in locally less organized water structures. Although the chaotropic nature of hydronium is under debate (e.g., (Tobias et al., 2009)), our results suggest that a concentration of 10^{-4} M of hydronium ions facilitates the rearrangement of water clusters and favors their partitioning to the membrane, resulting in reduced partition energy values (Fig. 1d).

3.2. *Partition energy of inorganic salts*

The affinities of various inorganic salts to the membrane were assessed by measuring both the energy of partition of each salt and its ability to neutralize the membrane surface charge (Fig. 2). To evaluate the mass added to the polyamide resulting solely from salt partitioning, we developed an experimental protocol and calculation procedure

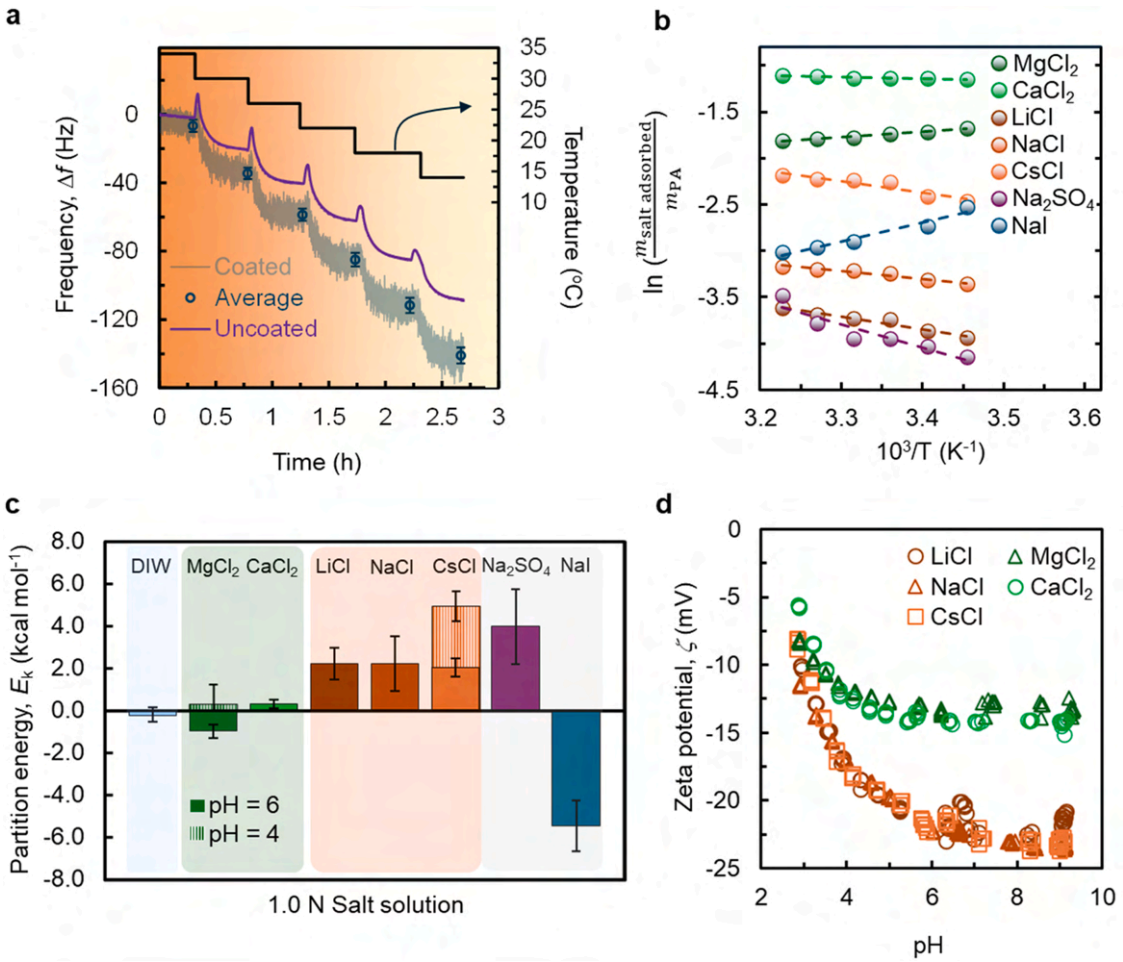

Fig. 2. QCM measurements of salt partition energies. (a) Representative raw frequency results for a polyamide (SW30HR)-coated sensor and uncoated sensor showing the effect of temperature on CsCl partitioning. Dark blue circles represent the average frequency over the final three minutes of each temperature, following system stabilization at each step, with the corresponding standard deviations. (b) Representative linearization of the van't Hoff equation (Eq. (S6)) for different salt solutions. (c) Average partition energy ($n \geq 3$) computed from the slopes of Eq. (S6) for water and various salts. Experimental conditions: 1.0 eq/L, pH = 6.0 and 4.0 (solid fill and striped fill, respectively), and descending temperature. (d) Zeta potential (ζ) measurements at different pH using single salt solutions of 1.0 mN chloride-salts (LiCl, NaCl, CsCl, $MgCl_2$, and $CaCl_2$) at 23 ± 0.8°C. The error bars represent standard deviation.

elaborated in the Supplementary Material. The overall mass increase resulting from solution filling the voids, and from ions and water partitioning to the polyamide led to QCM frequency decrease (Fig. 2a). Fig. 2a shows that the frequency of salt solutions oscillates considerably, presumably as a result of tiny fluctuations in the state of the system at dynamic equilibrium between the solution and the polyamide that occur at the molecular level at very short time scales.

To quantitatively determine the partition enthalpy (referred to here, for simplicity, as partition energy) of each tested salt, we used the frequencies in Figs. 1b and 2a to compute the ratio of adsorbed salt mass to polyamide mass. This ratio equals to the partition coefficient multiplied by a constant (Eq. (S5)) and was analyzed as a function of temperature. Based on this data, we attained the linearization of van't Hoff equation (Eq. (S7) and Fig. 2b) that shows negative slopes for ions with lower affinity to the membrane and positive slopes for ions with higher affinity to the membrane (compared to the solution). As detailed in the SI, the exact value of the partition coefficient is not required to determine the slopes, i.e., the partition energy. This is advantageous, as an exact calculation of K would necessitate knowledge of the number of water molecules coordinated to the partitioned ion, which is unavailable. Instead, the slope calculation relies solely on the assumption that the ion's coordination number remains constant across the tested temperature range. Note that as the same equivalent concentration was used for all experiments with chloride-based salts, the molar concentration of chloride was kept constant. Therefore, it is assumed that chloride partitioning is relatively consistent across the five salts, allowing the resultant slopes and E_k values to be used for comparing the associated cations. Similarly, the sodium concentration was the same for sodium-based salts, allowing for comparing the anions.

The calculated partition energies for the tested salts (Table 1) are slightly lower than previously reported effective energy barriers for salt permeabilities through the SW30 membrane (Shefer et al., 2022). This relation underscores the link between partition energy and the effective energy barrier of permeability; that is, the partition energy is part of (and therefore lower than) the effective energy barrier of the permeability for a given scenario. Apparently, no significant differences were observed between E_k of the monovalent chloride salts (LiCl, NaCl, and CsCl), albeit their differences in hydration enthalpy and size (Table 1). We suspect that the QCM methodology is not sensitive enough to detect the minor differences between these salts (as observed also in the ZP measurements, Fig. 2d). However, a clear distinction is observed when comparing the two groups of chloride salts – alkali metal (X^+) and alkaline earth metal (X^{2+}) salts. The latter group, represented by Ca^{2+} and Mg^{2+}, exhibits significantly lower partition energies compared to the former group (i.e., Li^+, Na^+, and Cs^+). Despite the non-negligible formation of ion pairs in solution (e.g., $MgCl^+$), which reduces the concentration of free divalent cations, the low (and even negative) partition energies of the divalent cations can be attributed to their

Table 1
Main properties of the ions investigated in this study.

Ion	Crystal radius (Å) (Nightingale, 1959)	Hydrated radius (Å) (Nightingale, 1959)	Hydration enthalpy (kcal mol^{-1}) (Marcus, 1994)	Polarizability (Å^3) (Molina et al., 2012)
Lithium (Li^+)	0.60	3.82	-126.8	0.029
Sodium (Na^+)	0.95	3.58	-99.29	0.18
Cesium (Cs^+)	1.69	3.29	-66.99	2.02
Magnesium (Mg^{2+})	0.65	4.28	-464.86	0.08
Calcium (Ca^{2+})	0.99	4.12	-382.41	0.44
Chloride (Cl^-)	1.81	3.32	-76.04	3.5
Iodide (I^-)	2.16	3.31	-69.3	7.5
Sulfate (SO_4^{2-})	2.90	3.79	-247.4	-

higher electrostatic-based affinity to the membrane. Acknowledging that the measured E_k represents a complex contribution of partition energies from all species present in the solution, we infer that the partition energy of divalent cations to a negatively charged membrane (i.e., at pH = 6.0) is considerably lower than that of monovalent cations, thus dominating and lowering the overall measured E_k. Notably, while the QCM tests were performed at high salt concentration, which induces screening of the negatively charged carboxyl groups in the polyamide layer, it was previously shown that the polyamide layer maintains its negative charge even under very high salt concentration (Coday et al., 2015), corroborating the idea that electrostatic interactions can explain the lower partition energies observed for divalent cations. This idea is supported by the higher E_k values of the magnesium and cesium cations measured for a less negatively charged membrane at pH 4.0 (striped fill in Fig. 2c). Comparing E_k of iodide and sulphate reveals that I^-, being a monovalent, large, weakly hydrated, highly polarizable, and chaotropic ion (Table 1), thermodynamically favors the interactions with the membrane over its interactions with water (Shefer et al., 2025). On the other hand, the divalent and strong kosmotropic (i.e., water structure maker) SO_4^{2-} is strongly repelled from the negatively charged membrane, making its partition energy relatively high.

Our zeta potential results support the interpretation that symmetric monovalent salts (LiCl, NaCl, and CsCl) show almost identical affinities towards the membrane while the divalent cation-based salts ($CaCl_2$ and $MgCl_2$) exhibit higher affinity towards the membrane (Fig. 2d). This difference in the affinities of the two groups of ions is reflected by the more substantial neutralization of membrane charge by the divalent cations compared to the monovalent cations – where for pH > 6.0, divalent cations lead to ζ of approximately -14 mV, while monovalent ions lead to ζ of approximately -23 mV, although their charge-equivalent concentrations (N) were identical. Moreover, at slightly acidic conditions, i.e., at pH = 4.5, where the concentration of hydronium is merely 3% of the concentration of the cation, the $|\zeta|$ of the monovalent cation solutions is significantly reduced compared to $|\zeta|$ at neutral conditions. In other words, the affinity of hydronium ion to the membrane is probably higher than the affinity of the tested monovalent cations, leading to better neutralization by H^+ than by Cs^+, Na^+, or Li^+. However, the same concentration of H^+ hardly affects the ζ in the case of the divalent cation solutions, showing a constant ζ for 4.5 < pH < 9.0, which indicates the high affinity to the membrane of divalent cations.

3.3. Correlation between the partition energy and salt permeability

In a last set of experiments, we examined the link between salt partition enthalpy (E_k) and salt permeability (B) to better understand the role of partition enthalpy in the transport (Fig. 3). Our results indicate that there is no single relationship between B and E_k for the tested ions, implying that intrapore diffusion barriers or entropic effects during partitioning can govern the salt permeability in certain cases (Fig. 3a and S2). Notably, while within each group of cations (i.e., monovalent or divalent) relatively similar B and E_k values are exhibited, comparing the results of monovalent and divalent cations reveals a direct relationship between B and E_k; that is, the divalent cations, which have lower E_k values, have lower B values compared to the monovalent cations, which have higher E_k and higher B values. This trend is likely due to the more enthalpically hindered intrapore diffusion of the divalent cations resulting from the stronger interactions that these cations form with the negatively charged carboxyl groups compared to the monovalent cations. In contrast, an opposite trend is evident for the anions, where the divalent sulphate anion with higher partition enthalpy shows lower permeability compared to the monovalent iodide and chloride anions, likely due to the higher repulsion of sulphate from the membrane.

Notably, while the partition energies of Mg^{2+} and Cs^+ were both increased under conditions of less negative membrane charge (Fig. 2c), their permeabilities were oppositely affected (Fig. 3a), further highlighting the critical role of intrapore diffusion in the transport. Overall, our results suggest that for cations, which form favorable interactions with the negatively charged membrane, an inverse relationship exists between partition energy and the energy barrier for diffusion within the membrane, as stronger interactions between the ion and the membrane enhance ion partitioning but hinder its intrapore diffusion (Fig. 3b). However, for the anions, such an inverse relationship is less notable. Nevertheless, iodide and chloride, despite having significantly different E_k values, show similar B values, possibly due to a tradeoff between their partitioning and intrapore diffusion, as discussed for the cations. Specifically, iodide is a large hydrophobic and highly polarizable anion that can readily undergo dehydration at the pore mouth and then stick to the membrane pore with the resulting lower intrapore diffusion. Sulphate, on the other hand, has the highest E_k (at pH 6) and the lowest B value among the tested salts, which obscure our understanding whether its intrapore diffusion is slower or faster compared to the other anions.

4. Conclusions

Our study highlights the pivotal link between partition energies and the interactions formed between inorganic ions and polyamide membranes. The findings demonstrate significant water uptake by the membrane, indicating the membrane's strong affinity to water, presumably driven by dipole interactions and hydrogen bonding. The partition energies of various salts revealed distinct behaviors for monovalent and divalent cations, which interestingly correlate with their respective permeability trends. While monovalent cations showed similar E_k values (implying on their similar affinities to the membrane), divalent cations displayed stronger interactions with the membrane, resulting in lower partition energies. Nevertheless, the permeability rates of the divalent cations were lower than those of the monovalent cations, probably due to the slower intrapore diffusion of the divalent cations. Anions, particularly iodide and sulphate, illustrated contrasting partition energy-permeability trends, influenced by their valency, size, and likely their chaotropic/kosmotropic nature. Overall, our investigation provides a deeper understanding of ion transport and ion-membrane interactions, underscoring the intricate balance between partitioning and intrapore diffusion that governs ion permeability. The results of this research set the foundations for future exploration on molecular mechanisms governing ion-specific interactions and their implications for membrane design in ion-ion selective separation processes.

CRediT authorship contribution statement

Liat Birnhack: Writing – review & editing, Writing – original draft,

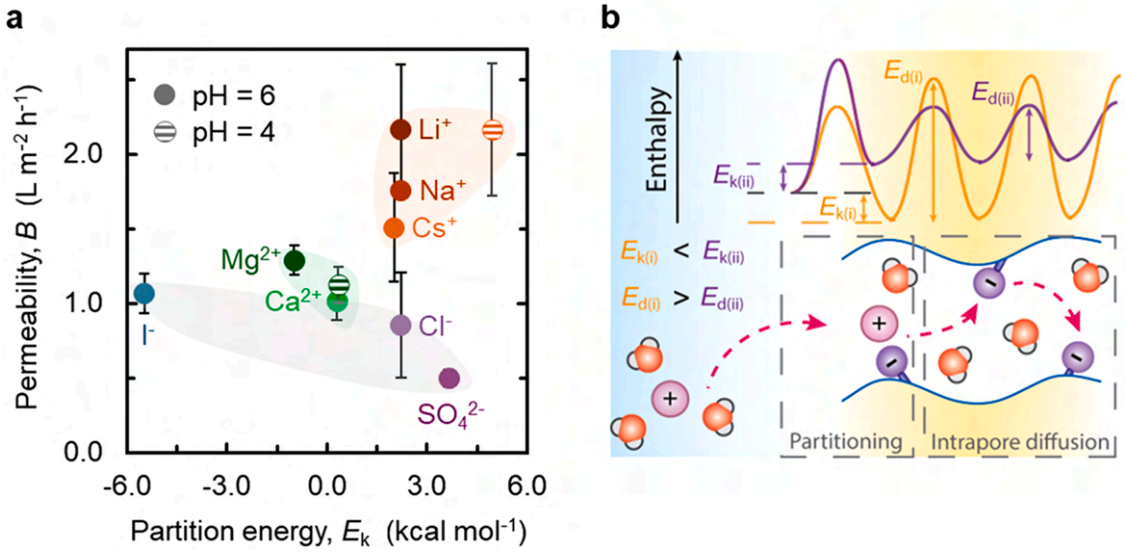

Fig. 3. Correlation between solute partition energy and permeability. (a) Results of filtration experiments performed under the following conditions: pressure of 10 bar, crossflow velocity of 2.13 m s^{-1}, concentration of 2.0 mN for each salt, and pH 6.0 (full symbols) and 4.0 (striped symbols representing Mg^{2+} and Cs^{+}). Monovalent cations and divalent cations are represented by orange and green color scales, respectively. (b) Schematic of the enthalpy landscape for two cations permeating the membrane: a cation with higher affinity to the membrane (i.e., lower E_k) shows higher energy barrier for intrapore diffusion (E_d) compared to a cation with lower affinity to the membrane (i.e., higher E_k). Pink sphere with '+' sign and purple spheres with '-' sign represent solution cations and carboxyl groups of the polyamide layer, respectively. The error bars represent standard deviation.

Validation, Methodology, Investigation, Formal analysis, Conceptualization. **Oren Ben Porat:** Methodology, Investigation, Formal analysis, Conceptualization. **Ori Fridman:** Methodology, Investigation, Formal analysis. **Tiezheng Tong:** Writing – review & editing, Visualization, Funding acquisition. **Razi Epsztein:** Writing – review & editing, Visualization, Supervision, Resources, Methodology, Funding acquisition, Formal analysis, Conceptualization.

Declaration of competing interest

The authors declare the following financial interests/personal relationships which may be considered as potential competing interests:

Razi Epsztein reports financial support was provided by Israel Science Foundation. Razi Epsztein reports financial support was provided by United States-Israel Binational Science Foundation. Tiezheng Tong reports financial support was provided by National Science Foundation. If there are other authors, they declare that they have no known competing financial interests or personal relationships that could have appeared to influence the work reported in this paper.

Acknowledgements

This work was supported by the Israel Science Foundation (grant No. 1269/21), a grant from the United States – Israel Binational Science Foundation (BSF), Jerusalem, Israel (grant No. 2023653), and a grant from the United States National Science Foundation (grant No. 2448410).

Supplementary materials

Supplementary material associated with this article can be found, in the online version, at doi:10.1016/j.memlet.2025.100099.

Data availability

Data will be made available on request.

References

Allouzi, M., Avidar, M., Birnhack, L., Epsztein, R., Straub, A.P., 2025. Reliable methods to determine experimental energy barriers for transport in salt-rejecting membranes. J. Membr. Sci. Lett. 5. https://doi.org/10.1016/j.memlet.2024.100090.

Arrizabalaga, J., Rafaniello, I., Schäfer, T., 2025. Practical limits of the quartz crystal microbalance and surface plasmon resonance for elucidating salt or ion partitioning into membrane polymers. J. Memb. Sci. 713. https://doi.org/10.1016/j.memsci.2024.123348.

Bannon, S.M., Geise, G.M., 2024. Application of the born model to describe salt partitioning in hydrated polymers. ACS Macro Lett. 13, 515–520. https://doi.org/10.1021/acsmacrolett.4c00048.

Bannon, S.M., Kutner, E., Garretson, B., Geise, G.M., 2024. Understanding the influence of sodium chloride concentration on ion diffusion in charged polymers. J. Memb. Sci. 712. https://doi.org/10.1016/j.memsci.2024.123197.

Broadwater, T.L., Murphy, T.J., Evans, D.F., 1976. Conductance of binary asymmetric electrolytes in methanol. J. Phys. Chem. 80, 753–757. https://pubs.acs.org/sharingguidelines.

Chen, D., Werber, J.R., Zhao, X., Elimelech, M., 2017. A facile method to quantify the carboxyl group areal density in the active layer of polyamide thin-film composite membranes. J. Memb. Sci. 534, 100–108. https://doi.org/10.1016/j.memsci.2017.04.001.

Chen, X., Boo, C., Yip, N.Y., 2021. Influence of solute molecular diameter on permeability-selectivity tradeoff of thin-film composite polyamide membranes in aqueous separations. Water Res. 201. https://doi.org/10.1016/j.watres.2021.117311.

Coday, B.D., Luxbacher, T., Childress, A.E., Almaraz, N., Xu, P., Cath, T.Y., 2015. Indirect determination of zeta potential at high ionic strength: specific application to semipermeable polymeric membranes. J. Memb. Sci. 478, 58–64. https://doi.org/10.1016/j.memsci.2014.12.047.

Drazevic, E., Bason, S., Kosutic, K., Freger, V., 2012. Enhanced partitioning and transport of phenolic micropollutants within polyamide composite membranes. Env. Sci. Technol. 46. https://doi.org/10.1021/es204188j.

Dunmyer, M., Welchert, J., Bellido-Aguilar, D.A., Brusseau, M., Savagatrup, S., Karanikola, V., 2024. Molecular scale adsorption behavior of per- and polyfluoroalkyl substances (PFAS) on model surfaces. Chem. Eng. J. 497. https://doi.org/10.1016/j.cej.2024.154286.

Epsztein, R., 2022. Intrinsic limitations of nanofiltration membranes to achieve precise selectivity in water-based separations. Front. Membr. Sci. Technol 1. https://doi.org/10.3389/frmst.2022.1048416.

Fan, H., Heiranian, M., Elimelech, M., 2024. The solution-diffusion model for water transport in reverse osmosis: what went wrong? Desalination 580. https://doi.org/10.1016/j.desal.2024.117575.

Fisher, F.H., Fox, A.P., 1975. NaSO4- Ion pairs in aqueous solutions at pressures up to 2000 atm. J. Solut. Chem. 4, 225–236.

Freger, V., 2004. Swelling and morphology of the skin layer of polyamide composite membranes: an atomic force microscopy study. Env. Sci. Technol. 38, 3168–3175. https://doi.org/10.1021/ES034815U.

Freger, V., 2023. Dielectric exclusion, an éminence grise. Adv. Colloid. Interface Sci. 319. https://doi.org/10.1016/j.cis.2023.102972.

Gao, W., She, F., Zhang, J., Dumée, L.F., He, L., Hodgson, P.D., Kong, L., 2015. Understanding water and ion transport behaviour and permeability through poly (amide) thin film composite membrane. J. Memb. Sci. 487. https://doi.org/10.1016/j.memsci.2015.03.052.

Geise, G.M., Paul, D.R., Freeman, B.D., 2014. Fundamental water and salt transport properties of polymeric materials. Prog. Polym. Sci. 39, 1–24. https://doi.org/10.1016/j.progpolymsci.2013.07.001.

Ghoufi, A., Dražević, E., Szymczyk, A., 2017. Interactions of organics within hydrated selective layer of reverse osmosis desalination membrane: a combined experimental and computational study. Env. Sci Technol 51. https://doi.org/10.1021/acs.est.6b05153.

Heiranian, M., Duchanois, R.M., Ritt, C.L., Violet, C., Elimelech, M., 2022. Molecular simulations to elucidate transport phenomena in polymeric membranes. Env. Sci. Technol. 56. https://doi.org/10.1021/acs.est.2c00440.

Heiranian, M., Fan, H., Wang, L., Lu, X., Elimelech, M., 2023. Mechanisms and models for water transport in reverse osmosis membranes: history, critical assessment, and recent developments. Chem. Soc. Rev. 52. https://doi.org/10.1039/d3cs00395g.

Hu, Y., Wang, F., Yang, Z., Tang, C.Y., 2023. Modeling nanovoid-enhanced water permeance of thin film composite membranes. J. Memb. Sci. 675. https://doi.org/10.1016/j.memsci.2023.121555.

Jin, P., Chergaoui, S., Zheng, J., Volodine, A., Zhang, X., Liu, Z., Luis, P., Van der Bruggen, B., 2022. Low-pressure highly permeable polyester loose nanofiltration membranes tailored by natural carbohydrates for effective dye/salt fractionation. J. Hazard. Mater. 421. https://doi.org/10.1016/j.jhazmat.2021.126716.

Kimani, E.M., Kemperman, A.J.B., Van Der Meer, W.G.J., Biesheuvel, P.M., 2021. Multicomponent mass transport modeling of water desalination by reverse osmosis including ion pair formation. J. Chem. Phys. 154. https://doi.org/10.1063/5.0039128.

Kingsbury, R.S., Baird, M.A., Zhang, J., Patel, H.D., Baran, M.J., Helms, B.A., Hoek, E.M. V., 2024. Kinetic barrier networks reveal rate limitations in ion-selective membranes. Matter 7, 2161–2183. https://doi.org/10.1016/J.MATT.2024.03.021.

Lin, L., Weigand, T.M., Farthing, M.W., Jutaporn, P., Miller, C.T., Coronell, O., 2018. Relative importance of geometrical and intrinsic water transport properties of active layers in the water permeability of polyamide thin-film composite membranes. J. Memb. Sci. 564, 935–944. https://doi.org/10.1016/j.memsci.2018.08.002.

Mai, Z., Gui, S., Fu, J., Jiang, C., Ortega, E., Zhao, Y., Tu, W., Mickols, W., Van der Bruggen, B., 2019. Activity-derived model for water and salt transport in reverse osmosis membranes: a combination of film theory and electrolyte theory. Desalination 469. https://doi.org/10.1016/j.desal.2019.114094.

Y. Marcus, A simple empirical model describing the thermodynamics of hydration of ions of widely varying charges, sizes, and shapes, c (1994) 111–127.

J.J. Molina, S. Lectez, S. Tazi, M. Salanne, J. Dufrèche, J. Roques, P.A. Madden, P. Turq, J.J. Molina, S. Lectez, S. Tazi, M. Salanne, Ions in solutions : determining their polarizabilities from first-principles Ions in solutions : determining their polarizabilities from first-principles, 014511 (2012). https://doi.org/10.1063/1.3518101.

Nickerson, T.R., Antonio, E.N., McNally, D.P., Toney, M.F., Ban, C., Straub, A.P., 2022. Unlocking the potential of polymeric desalination membranes by understanding molecular-level interactions and transport mechanisms. Chem. Sci. 14. https://doi.org/10.1039/d2sc04920a.

Nightingale, E.R., 1959. Phenomenological theory of ion solvation. Effective radii of hydrated ions. J. Phys. Chem. 63. https://doi.org/10.1021/j150579a011.

Oren, Y.S., Freger, V., Nir, O., 2021. Journal of Membrane Science Letters new compact expressions for concentration-polarization of trace-ions in pressure-driven membrane processes. J. Membr. Sci. Lett. 1, 100003. https://doi.org/10.1016/j.memlet.2021.100003.

Paul, D.R., 2004. Reformulation of the solution-diffusion theory of reverse osmosis. J. Memb. Sci. 241. https://doi.org/10.1016/j.memsci.2004.05.026.

Pavluchkov, V., Shefer, I., Peer-Haim, O., Blotevogel, J., Epsztein, R., 2022. Indications of ion dehydration in diffusion-only and pressure-driven nanofiltration. J. Memb. Sci. 648, 120358. https://doi.org/10.1016/j.memsci.2022.120358.

Razmjou, A., Asadnia, M., Hosseini, E., Habibnejad Korayem, A., Chen, V., 2019. Design principles of ion selective nanostructured membranes for the extraction of lithium ions. Nat Commun 10. https://doi.org/10.1038/s41467-019-13648-7.

Rickman, M., Davis, R.H., Pellegrino, J., 2014. Temperature-variation study of neutral solute and electrolyte fractionation through cellulose acetate and polyamide membranes. J. Memb. Sci. 461. https://doi.org/10.1016/j.memsci.2014.03.023.

Ridgway, H.F., Orbell, J., Gray, S., 2017. Molecular simulations of polyamide membrane materials used in desalination and water reuse applications: recent developments and future prospects. J. Memb. Sci. 524. https://doi.org/10.1016/j.memsci.2016.11.061.

Roth, R.S., Birnhack, L., Avidar, M., Hjelvik, E.A., Straub, A.P., Epsztein, R., 2024. Effect of solution ions on the charge and performance of nanofiltration membranes. NPJ Clean Water 7. https://doi.org/10.1038/s41545-024-00322-9.

Roth, R.S., Birnhack, L., Avidar, M., Hjelvik, E.A., Straub, A.P., Epsztein, R., 2024. Effect of solution ions on the charge and performance of nanofiltration membranes. NPJ Clean Water. 7. https://doi.org/10.1038/s41545-024-00322-9.

Schwindt, N.S., Avidar, M., Epsztein, R., Straub, A.P., Shirts, M.R., 2024. Interpreting effective energy barriers to membrane permeation in terms of a heterogeneous energy landscape. J. Memb. Sci. 712. https://doi.org/10.1016/j.memsci.2024.123233.

Shefer, I., Peer-Haim, O., Leifman, O., Epsztein, R., 2021. Enthalpic and entropic selectivity of water and small ions in polyamide membranes. Env. Sci. Technol. 55. https://doi.org/10.1021/acs.est.1c04956.

Shefer, I., Lopez, K., Straub, A.P., Epsztein, R., 2022. Applying transition-State theory to explore transport and selectivity in salt-rejecting membranes: a critical review. Env. Sci Technol. 56. https://doi.org/10.1021/acs.est.2c00912.

Shefer, I., Peer-Haim, O., Epsztein, R., 2022. Limited ion-ion selectivity of salt-rejecting membranes due to enthalpy-entropy compensation. Desalination 541. https://doi.org/10.1016/j.desal.2022.116041.

Shefer, I., Birnhack, L., Epsztein, R., 2025. The importance of ionic hydration in the transport of monovalent anions through nanofiltration membranes. J. Memb. Sci. 716. https://doi.org/10.1016/j.memsci.2024.123513.

Shin, M.G., Choi, W., Park, S.J., Jeon, S., Hong, S., Lee, J.H., 2022. Critical review and comprehensive analysis of trace organic compound (TOrC) removal with polyamide RO/NF membranes: mechanisms and materials. Chem. Eng. J. 427. https://doi.org/10.1016/j.cej.2021.130957.

Sujanani, R., Landsman, M.R., Jiao, S., Moon, J.D., Shell, M.S., Lawler, D.F., Katz, L.E., Freeman, B.D., 2020. Designing Solute-tailored selectivity in membranes: perspectives for water reuse and resource recovery. ACS Macro Lett 9, 1709–1717. https://doi.org/10.1021/acsmacrolett.0c00710.

Sujanani, R., Nordness, O., Miranda, A., Katz, L.E., Brennecke, J.F., Freeman, B.D., 2023. Accounting for ion pairing effects on sulfate salt sorption in cation exchange membranes. J. Phys. Chem. B 127, 1842–1855. https://doi.org/10.1021/acs.jpcb.2c07900.

Tang, C., Bruening, M.L., 2020. Ion separations with membranes. J. Polym. Scie 58, 2831–2856. https://doi.org/10.1002/pol.20200500.

Tobias, D.J., Sengupta, N., Beattie, J.K., Djerdjev, A.M., Link, G.G, O., Vöhringer-martinez, E., Liu, Y., Siefermann, K., Willard, A.P., Chandler, D., 2009. This paper is published as part of Faraday Discussions volume 141 : water – From interfaces to the bulk. Faraday Discuss 141.

Tu, K.L., Nghiem, L.D., Chivas, A.R., 2011. Coupling effects of feed solution pH and ionic strength on the rejection of boron by NF/RO membranes. Chem. Eng. J. 168. https://doi.org/10.1016/j.cej.2011.01.101.

Vickers, R., Weigand, T.M., Coronell, O., Miller, C.T., 2025. Water transport mechanisms during pressure-driven transport through polyamide nanogaps. Phys. Fluids 37. https://doi.org/10.1063/5.0248257.

Villalobos, L.F., Pataroque, K.E., Pan, W., Cao, T., Kaneda, M., Violet, C., Ritt, C.L., Hoek, E.M.V., Elimelech, M., 2023. Orientation matters: measuring the correct surface of polyamide membranes with quartz crystal microbalance. J. Membr. Sci. Lett. 3. https://doi.org/10.1016/j.memlet.2023.100048.

Wang, R., Lin, S., 2021. Pore model for nanofiltration: history, theoretical framework, key predictions, limitations, and prospects. J. Memb. Sci. 620, 118809. https://doi.org/10.1016/j.memsci.2020.118809.

Wang, J., Mo, Y., Mahendra, S., Hoek, E.M.V., 2014. Effects of water chemistry on structure and performance of polyamide composite membranes. J. Memb. Sci. 452. https://doi.org/10.1016/j.memsci.2013.09.022.

Wang, J., Kingsbury, R.S., Perry, L.A., Coronell, O., 2017. Partitioning of Alkali metal salts and boric acid from aqueous phase into the polyamide active layers of reverse osmosis membranes. Env. Sci Technol. 51, 2295–2303. https://doi.org/10.1021/acs.est.6b04323.

Wang, L., Cao, T., Dykstra, J.E., Porada, S., Biesheuvel, P.M., Elimelech, M., 2021. Salt and water transport in reverse osmosis membranes: beyond the solution-diffusion model. Env. Sci. Technol. 55, 16665–16675. https://doi.org/10.1021/acs.est.1c05649.

Wang, J., Armstrong, M.D., Grzebyk, K., Vickers, R., Coronell, O., 2021. Effect of feed water pH on the partitioning of alkali metal salts from aqueous phase into the polyamide active layers of reverse osmosis membranes. Env. Sci Technol. 55, 3250–3259. https://doi.org/10.1021/acs.est.0c06140.

Wang, R., Zhang, J., Tang, C.Y., Lin, S., 2022. Understanding selectivity in solute–Solute separation: definitions, measurements, and comparability. Env. Sci. Technol. https://doi.org/10.1021/acs.est.1c06176.

Wang, L., He, J., Heiranian, M., Fan, H., Song, L., Li, Y., Elimelech, M., 2023. Water transport in reverse osmosis membranes is governed by pore flow, not a solution-diffusion mechanism. Sci. Adv. 9. https://doi.org/10.1126/sciadv.adf8488.

Wijmans, J.G., Baker, R.W., 1995. The solution-diffusion model: a review. J. Memb. Sci. 107. https://doi.org/10.1016/0376-7388(95)00102-I.

Yaroshchuk, A., Bruening, M.L., Licón Bernal, E.E., 2013. Solution-Diffusion-Electro-Migration model and its uses for analysis of nanofiltration, pressure-retarded osmosis and forward osmosis in multi-ionic solutions. J. Memb. Sci. 447, 463–476. https://doi.org/10.1016/j.memsci.2013.07.047.

Yaroshchuk, A.E., 2001. Non-steric mechanism of nanofiltration: superposition of donnan and dielectric exclusion. Sep. Purif. Technol. 22–23, 143–158. https://doi.org/10.1016/S1383-5866(00)00159-3.

Yazzie, C.B., Elias, C., Karanikola, V., 2024. Uranium rejection with nanofiltration membranes and the influence of environmentally relevant mono- and divalent cations at various pH. Env. Sci. (Camb). https://doi.org/10.1039/d4ew00324a.

Zhao, Y., Tong, T., Wang, X., Lin, S., Reid, E.M., Chen, Y., 2021. Differentiating solutes with precise nanofiltration for next generation environmental separations: a review. Env. Sci Technol 55. https://doi.org/10.1021/acs.est.0c04593.

Zhou, X., Wang, Z., Epsztein, R., Zhan, C., Li, W., Fortner, J.D., Pham, T.A., Kim, J.H., Elimelech, M., 2020. Intrapore energy barriers govern ion transport and selectivity of desalination membranes. Sci. Adv. 6. https://doi.org/10.1126/sciadv.abd9045.

Zhu, X., Leininger, A., Jassby, D., Tsesmetzis, N., Ren, Z.J., 2021. Will membranes break barriers on volatile fatty acid recovery from Anaerobic digestion? ACS ES T Eng. 1. https://doi.org/10.1021/acsestengg.0c00081.